Pediatr Radiol (2016) 46:941–951
DOI 10.1007/s00247-014-3204-9

MINISYMPOSIUM: PEDIATRIC MR SPECTROSCOPY

# Key concepts in MR spectroscopy and practical approaches to gaining biochemical information in children

**Loukas G. Astrakas · Maria I. Argyropoulou**

Received: 26 February 2014 / Revised: 11 September 2014 / Accepted: 1 October 2014


**Abstract** Magnetic resonance spectroscopy (MRS) provides independent biochemical information and has become an invaluable adjunct to MRI and other imaging modalities. This review introduces key concepts and presents basic methodological steps regarding the acquisition and the interpretation of proton MRS. We review major brain metabolites and discuss MRS dependence on age, location, echo time and field strength.

**Keywords** Magnetic resonance spectroscopy · Chemical shift · J-coupling · Metabolites · Central nervous system · Children

## Introduction

Nuclear magnetic resonance, since its discovery in 1946, has been developed into a widespread, versatile scientific tool with substantial impact on the natural sciences. It is based on the interactions of radiowaves with nuclear spins in the presence of a magnetic field. The measurement of these interactions offers valuable structural and dynamic information at the molecular level, thus establishing nuclear MR as one of the most powerful techniques of analytical and structural chemistry. A few decades after its invention, nuclear MR was applied in vivo in the form of magnetic resonance imaging (MRI) and magnetic resonance spectroscopy (MRS) [1]. Both use the spin of hydrogen nucleus $^{1}H$, (i.e. proton) because of its high natural abundance in the human body and its high magnetic sensitivity. In MRI high spatial resolution is required, so all hydrogen nuclei are treated collectively and structural information at the molecular level is lost. On the other hand, in proton MRS, spatial resolution is partly sacrificed in order to separate hydrogen nuclei according to their chemical group (moiety). Thus MRS can detect chemical compounds, which are usually small bio-molecules called metabolites, because they participate in specific metabolic pathways. Quantification of metabolites provides noninvasively important biochemical information and characterizes certain tissue metabolic processes and their relationship to diseases.

Historically MRS followed MRI because technically it was more challenging and demanded higher and more homogeneous magnetic fields. Also, spectra provided by MRS did not easily fit the image-centered radiologic practice. Now technical advances and numerous studies have established the importance of MRS in clinical and research settings. In pediatrics, proton MRS is applied mostly to the brain, although in adults there are growing numbers of studies of other organs, such as breast and prostate [2]. The aim of this review is to introduce the basic principles and key methodological points of acquisition and interpretation of proton MRS spectra. There are excellent reviews in the literature for readers interested to clinical application of MRS [3–7].

L. G. Astrakas (✉)
Medical Physics, Medical School,
University of Ioannina,
P.O. Box 1186, Ioannina 45110, Greece
e-mail: astrakas@uoi.gr

M. I. Argyropoulou
Radiology, Medical School,
University of Ioannina,
Ioannina, Greece

## Basic principles

Every bare hydrogen nucleus (proton) inside an external magnetic field $B_o$ has a resonant frequency $\omega_o$, also called Larmor frequency. However protons are not isolated in human tissue but belong to a complex chemical environment that contains many additional sources of magnetic field. These sources modify the bare proton's Larmor frequency. MRS allows us

to detect these modifications and get valuable conclusions about the proton's chemical environment. Chemical shift and J-coupling are two key concepts in MRS that are related with the magnetic interaction in the proton's environment, originating from the surrounding electrons and the nearby nuclei, respectively.

## Chemical shift

The moving electrons surrounding a proton within a molecule generate a magnetic field in the opposite direction of $B_o$. As a result the effective magnetic field on the proton becomes lower than $B_o$ and the proton is said to be shielded by the electrons. In general, differences in the electronic environments cause protons to experience slightly different applied magnetic fields owing to the shielding effect of the induced electronic magnetic fields (Fig. 1).

Electronic shielding causes protons with different chemical environments to yield resonance frequencies slightly shifted from the basic Larmor frequency $\omega_o$. These deviations of resonant frequency are called chemical shifts because they depend on the local chemical environment. For practical reasons chemical shift measurements are not based on the resonance position of the bare proton. Instead they are measured from the resonance frequency of the reference substance tetramethylsilane (TMS), using the formula:

$$\delta(\text{ppm}) = 10^6 * (\omega\text{-}\omega_{TMS})/\omega_{TMS}$$

where δ is the chemical shift of a proton in a chemical group in parts per million (ppm) and $\omega$, $\omega_{TMS}$ are the resonance frequencies of the proton in the chemical group and the protons in tetramethylsilane, respectively (Fig. 2). The big advantage of the parts-per-million scale is that it does not depend on $B_o$ thus producing comparable MRS measurements regardless of scanner strength.

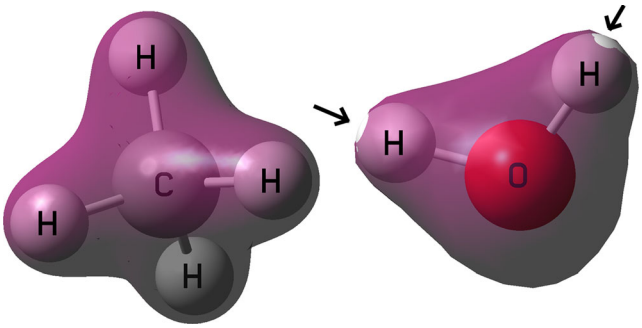


**Fig. 1** Electronic shielding in water and methane molecules. Electronic clouds (*purple*) in methane (*left*) and water molecules (*right*) depict 90% of the total electron density calculated using ab initio molecular simulation (Gaussian 03 W). Note the decreased electronic shielding of hydrogen atoms in the water molecule (*arrows*). Oxygen is more electronegative than carbon, meaning that it attracts stronger the electrons and leaves the H nuclei less shielded. Differences in electronic shielding result in differences in the magnetic field and thus differences in resonant frequencies between carbon's and oxygen's H atoms

In MRS spectra protons are separated in peaks according to their resonance frequencies or equivalently according to their chemical shift. Although often peaks are falsely associated with specific metabolites, in fact they correspond to protons belonging to the same or very similar chemical groups, hence called equivalent protons. As a result, different metabolites sharing the same moiety contribute to the same peak. An example is the trimethylamonium group N-$(CH_3)_3$, which resonates at 3.22 ppm. Conversely, metabolites with more than one chemical group often contribute to multiple peaks. An example is the contribution of creatine to 3.02 and 3.94 ppm peaks (Fig. 3).

## J-coupling

The magnetic field experienced by a single proton can be affected in multiple ways by nearby non-equivalent nuclei. When the proton is weakly coupled with nearby nuclei through three or fewer covalent bonds then its resonant peak splits into multiple components. This effect is called J-coupling or spin-spin coupling and its strength is represented by the so-called J-coupling constant J, measured in Hz. Note that J does not depend on the main field strength, although the peak splitting can be better detected in the improved spectral resolution of higher fields. In proton MRS, line splitting is very prominent in the case of lactate, where a doublet at 1.33 ppm arises from three magnetically equivalent methyl ($CH_3$) protons weakly coupled to the methine (CH) proton (Fig. 4).

## Methodology

There are many ways to perform and analyze MRS. None of them is considered universal or optimum. Even more important than the choice of a particular MRS protocol is the abiding attachment to it. MRS spectra are very sensitive to many experimental parameters and experience in MRS interpretation is better gained with consistent and comparable spectra obtained with the same protocol.

### Water suppression

MRS can detect small metabolites in the cell in millimolar concentrations. Their signal is typically several orders of magnitude smaller than the signal of water, which dominates the

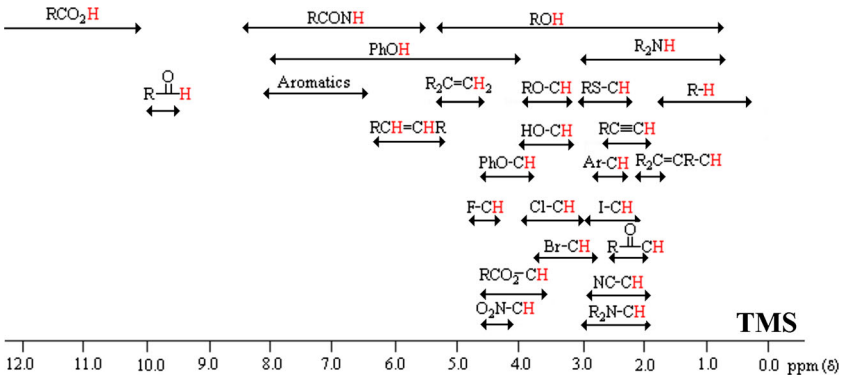


**Fig. 2** Proton resonance frequency ranges for various chemical groups

spectrum (Fig. 5) because of its high concentration (30–55 mol/L) in biological tissue. The large water signal makes it difficult — though not impossible — to obtain reliable parameter estimates for the low signal resonances of metabolites [8]. Most commonly water suppression methods are used to increase detection sensitivity of weak signal from metabolites, resulting in improved resolution and reduced measurement time (Fig. 5). Usually this is accomplished with a sequence of chemical-shift-selective-saturation (CHESS) 90° radiofrequency pulses and associated spoiling gradients that are used to excite and dephase water prior to the localization sequence [9]. Other approaches use frequency-selective radiofrequency pulses with different flip angles [10], or inversion recovery of the water signal [11].

## Localization

In MRS there are several techniques for acquisition from selected volumes within the body [12]. Generally they can be divided into single-voxel (or single-volume) and multi-voxel techniques. The most widely used single-voxel techniques are the point-resolved spectroscopy sequence (PRESS) and the stimulated echo acquisition mode (STEAM). They both employ a combination of three slice-selective excitations that intersect at the volume of interest. In the PRESS technique, a 90° excitation and two 180° refocusing pulses are used, whereas in the STEAM sequence all three pulses are 90° excitation pulses. Many studies have compared the clinical performances of PRESS and STEAM and have found differences in signal intensity, precision of volume selection, sensitivity to motion and diffusion, modulation from J-coupling, shortest attainable echo time, efficiency of water suppression and dependence on $B_1$ gradients [12].

Chemical shift imaging (CSI) is a multi-voxel technique that collects spectra from multiple adjacent volumes of interest in a single measurement [13–15]. Chemical shift imaging is also called spectroscopic imaging or magnetic resonance spectroscopic imaging. Spatial localization is achieved with

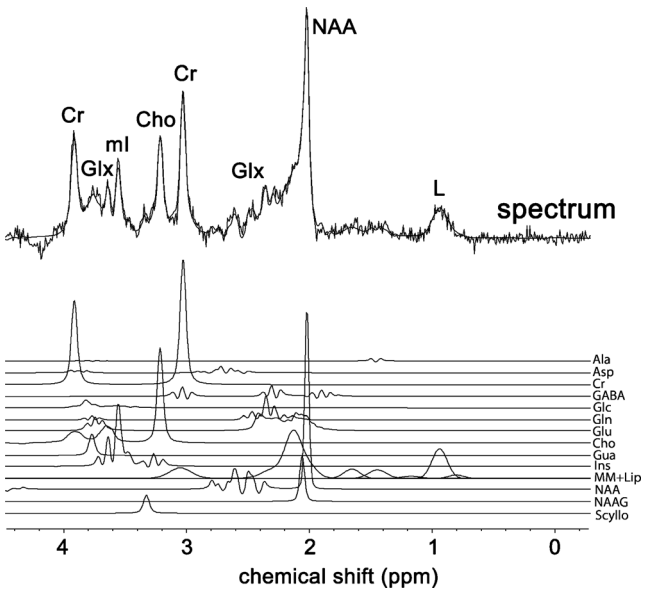


**Fig. 3** An adult proton brain spectrum obtained at an echo time (TE) of 30 ms and analyzed to its constituent metabolites

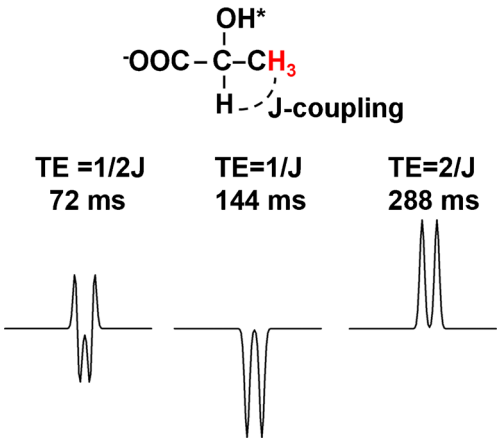


**Fig. 4** Echo time (TE) dependence. Methyl (*red*) of lactate creates a double peak because of J-coupling (=7 Hz) of methyl (*red*) protons with the methane proton (*dashed line*). For TE=72 ms doublets are out-of-phase; for TE=144 ms they are inverted (at 1.5 T); for TE=288 ms they are positive and in-phase

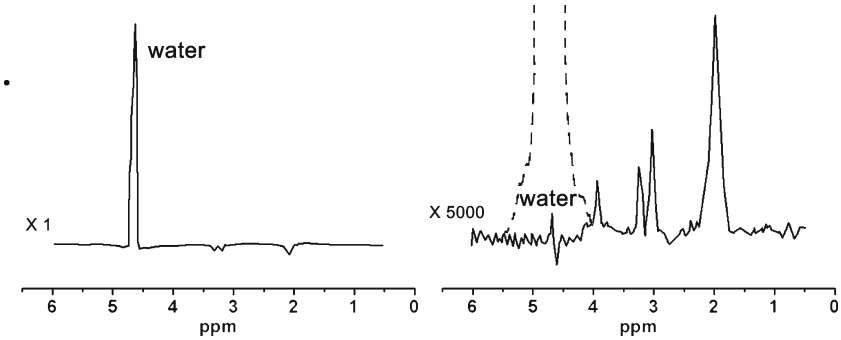


**Fig. 5** Proton spectrum with (*left*) and without (*right*) water suppression. *Dotted line* represents the water peak before suppression

phase encoding in one (1-D CSI), two (2-D CSI) and three (3-D CSI) dimensions as in standard MRI but with no readout gradient during data collection. Volume selective 2-D CSI, called also hybrid CSI, was developed to exclude undesired tissue (e.g., high lipid concentration, areas with susceptibility effect) that contaminates the adjacent spectra. This is attained by incorporating the volume selection pulses used in PRESS or STEAM single-voxel spectroscopy into the spectroscopic imaging sequence [16, 17]. Outer volume suppression is another way to avoid undesired signals in the spectrum and uses multiple saturation bands carefully placed around the volume of interest [16, 18].

Chemical shift imaging is preferable in non-local, diffuse or extended heterogeneous diseases where the spatial distribution of the metabolites is important. Unfortunately chemical shift imaging is often associated with reduced spectral resolution, chemical-shift artifact, voxel bleeding artifact (i.e. signal contamination into the voxel-of-interest from neighboring and even distant voxels) and voxel contamination from unsuppressed lipid or water signal. On the other hand single-voxel approaches are spatially limited but more robust and reproducible because of better magnetic field homogeneity and higher signal-to-noise ratio, resulting in well-defined peaks and uniform water suppression.

## Quantification

MRS quantification using mathematical processing calculates the contribution of each of the components of the MRS signal. The objective is to find all the peaks in the spectrum and calculate the areas under the peaks (not their heights!), also called peak intensities. The area under an MRS peak is proportional to the number of equivalent H nuclei contributing to this peak. The plurality and diversity of approaches for MRS quantification reflect the complexity of the subject [19–21]. Generally MRS quantification methods can be divided as follows:

(1) Absolute or relative quantification. Absolute quantification using a calibration procedure provides metabolite concentration in standard units (e.g., millimoles per kilogram wet weight), whereas relative quantification is based on metabolite ratios, often with total creatine as the denominator.
(2) Time or frequency domain. Time domain methods are applied on raw, unprocessed MRS data, whereas frequency domain methods are applied after the preprocessing stage, which typically includes apodization, zero filling, Fourier transform and phasing of the data.
(3) With or without prior knowledge. Methods with prior knowledge parameterize the MRS signal using information obtained by model spectra of metabolite solutions in vitro. Other automated, so-called black box methods directly estimate signal parameters without prior knowledge and often with minimal user interaction.

Many studies describe the relative advantages of each methodology [22, 23]. In practice, all modern scanners provide spectral quantification, but usually state-of-the-art methods like LCModel and jMRUI [24] require offline data processing. The majority of MRS studies are using relative quantification because it is faster and simpler, although it is not always accurate. Also changes of metabolite ratios are difficult to interpret because they can originate from changes of the numerator, denominator or both. Conversely, absolute quantification is in principle the right approach, but it requires extra scanning time and advanced post-processing, often becoming inefficient in clinical practice. Sometimes a good alternative for relative quantification is the comparison with spectra acquired at contra-lateral voxels in non-affected healthy tissue.

Often MR spectroscopy imaging quantification results are described by metabolite maps, which depict the spatial distribution of the metabolites. Although, for demonstration purposes, these maps appear smooth, essentially they have

resolution equal to the voxel dimensions of the MR spectroscopy imaging grid.

## Metabolites

Among the plethora of the metabolites in the brain, MRS can detect only few that have high concentrations and relaxation times within the detection range of current technology. Utilizing an intermediate to long (144–288 ms) echo time (TE) at 1.5 T, in most cases MRS can reliably detect N-acetylaspartate (NAA), choline-containing compounds (Cho), creatine and phosphocreatine (Cr) and lactate (Lac). For short TE (<40 ms) MRS can additionally detect myo-inositol (mI), glutamate and glutamine (Glx), glucose (Gc) and some macromolecules (e.g., proteins and lipids) (Fig. 3). Table 1 summarizes the most important brain metabolites detected by proton MRS.

### N-acetylaspartate (NAA)

N-acetylaspartate appears in the MRS spectra with a prominent peak at 2.01 ppm. Smaller contributions (<20%) to the same peak come from other neurochemicals containing the acetyl-group such as N-acetylaspartylglutamate (NAAG), N-acetylglutamate and N-acetylglucosamine. Although NAA has been found in immature oligodendrocytes and astrocyte progenitor cells, it is produced and stored almost exclusively in neurons. Specifically, NAA is synthesized from aspartate and acetyl-coenzyme-A in neuronal mitochondria. Its production is associated with fundamental metabolic processes such as the neuronal lipid synthesis via the adenosine triphosphate-citric lyase pathway and the energy production via the Krebs cycle. For all these reasons, NAA is considered a marker of neuronal density, function and viability. It decreases in cases of neuron loss, such as glioma, ischemia and degenerative diseases [25–28]. During development NAA is transported out of the neurons to the oligodendrocytes. There it is degraded to aspartate, which is used for myelin and lipid synthesis. NAA is also considered a neuronal osmolyte because of its high concentration in the brain parenchyma [29].

### Choline (Cho)

Choline-containing compounds peak at 3.22 ppm comprise metabolites with the trimethylamonium group N-$(CH_3)_3$. It is also referred to as choline, or total choline (tCho), or trimethylamines (TMA) peak. The main contributors of the peak are the intracellular pools of phosphocholine (PCho) and glycerophosphocholine (GPC), which play an important role in the phospholipid metabolism of cell membrane. Smaller contributions to the Cho peak originate from other trimethylamine compounds such as free choline, citidine diphosphate choline (CDP-Cho), acetylcholine and betaine. Cellular membrane turnover during cell proliferation in neoplasms and membrane disruption in demyelination result in Cho increase [28, 30].

### Creatine and phosphocreatine (Cr)

The methyl groups of creatine and phosphocreatine resonate at 3.02 ppm and are practically indistinguishable for magnetic fields lower than 7 T. A smaller peak at 3.94 ppm originates from the methylene groups. Creatine is synthesized in the human body from amino acids in the kidney, liver and pancreas. An active transmembrane creatine transporter helps creatine to enter the cells. Then, using excess adenosine

**Table 1** Common brain metabolites detected by proton magnetic resonance spectroscopy

| Metabolite | Concentration (mM) | Chemical shift (ppm) | Role |
|---|---|---|---|
| NAA | 7.8 | 2.01 | Neuronal marker, osmolyte |
| Cho | 1.5 | 3.22 | Marker of membrane turnover |
| Cr | 4.5 | 3.02, 3.94 | Marker of energetic status of cell |
| mI | | 3.56 (short TE) | Osmolyte, glial cell marker |
| Glx | 5–10 | 2.2–2.6<br>3.6–3.8 (short TE) | Neurotransmitters, markers of destructive neuronal process |
| Lac | 1 | 1.35±7 | Marker of anaerobic glycolysis |
| Lip | | 0.9, 1.3 (short TE) | Marker of apoptosis/necrosis |

*Cr* creatine and phosphocreatine, *Cho* choline, *Glx* glutamate and glutamine, *Lac* lactate, *Lip* lipids, *mI* myo-inositol, *NAA* N-acetylaspartate, *ppm* parts per million, *TE* echo time, *mM* millimolar

triphosphate it is converted to phosphocreatine, a high energy reserve that buffers cellular adenosine triphosphate/adenosine diphosphate reservoirs. Therefore the creatine peak is considered a marker of aerobic energy metabolism. The creatine peak has also been regarded as an internal standard because of the interconversion of creatine and phosphocreatine. However, in some cases (e.g., Cr deficiency syndromes, stroke, tumor and trauma) Cr has been found to decrease, whereas in others (e.g., trauma hyperosmolar cases) it has been found to increase [3, 31].

Lactate (Lac)

Lactate appears as a doublet peak at 1.33 ppm only in pathological conditions. Its shape depends on the echo time and usually it is detected at 1.5 T and at long echo times of 144 ms (at 1.5 T) or 288 ms (at 1.5 T and 3 T) where the adjacent lipid peaks are absent. Lactate is the end product of anaerobic glycolysis and therefore it is considered a marker of hypoxia or mitochondria dysfunction [32, 33]. It increases in stroke, high-grade tumors, abscesses, mitochondrial disorders, inflammatory response and macrophage infiltration [34–36]. In neonates, especially at 1.5 T, lactate can be confused with propylene glycol, a solvent in pentobarbital [37].

Myo-inositol (mI)

Myo-inositol is a pentose sugar visible at short echo time MRS spectra at 3.56 ppm. Other smaller contributors to the same peak are the inositol monophosphate and diphosphate and phosphatidyl inositol. Myo-inositol is an important cell osmotic regulator and also participates in the phosphoinositide signal transduction pathway. It is considered to be a glial marker because it is only present in glia. It increases in inflammatory disease from glial proliferation or increased glial cell size. It is also elevated in trauma [38] and some degenerative diseases (e.g., gliosis, astrocytosis, Alzheimer disease, dementia) [39]. It may be decreased in stroke, tumor, infection and low-grade malignancies [5].

Glutamate and glutamine (Glx)

At 2.2–2.6 and 3.6–3.8 ppm there are overlapping peaks of glutamate (Glu), glutamine (Gln), gamma-aminobutyric acid (GABA), aspartate and glucose. They are labeled as a composite peak Glx because it is difficult to separate them in MRS spectra, at least at 1.5 T. Glutamate is the most abundant neurotransmitter in the brain, located in neurons and to a lesser extent in glial cells. Glutamine is the primary derivative of glutamate and is present in astrocytes. They both participate in the detoxification and regulation of neurotransmitters. GABA is an important inhibitory neurotransmitter derived from glutamate. Glx peaks have been found to increase in hypoxic–ischemic injury, hepatic encephalopathies, schizophrenia and epilepsy [4].

Lipids (Lip)

In pathological conditions and with short echo times mobile lipid and macromolecule resonances become visible. Major peaks appear at 1.3 ppm for $(C\mathbf{H_2})_n$ and at 0.9 ppm for $C\mathbf{H_3}$, and smaller resonances appear at 2.05 ppm ($CH_2$-$C\mathbf{H_2}$-CH=), 2.2 ppm (−OOC-$C\mathbf{H_2}$-$CH_2$-) and 2.8 ppm (=CH$C\mathbf{H_2}$-CH=). They have been found in high-grade tumors, abscesses, acute inflammation and acute stroke. They are usually produced from cell membrane breakdown or from bacterial metabolism [40].

Other metabolites

Many metabolites (e.g., taurine, NAAG, scyllo inositol, ethanolamine, histidine, glycogen), usually with small contribution to the normal MRS spectrum, are practically undetectable. Some of them increase under disease conditions and thus can be quantified. Some examples include acetone, phenylalanine, succinate, pyruvate, alanine, glycine and threonine [41–44].

## Age and location dependence

A special difficulty on the interpretation of pediatric MRS is the variation of metabolite concentration during brain development (Fig. 6). Several studies have provided normative curves describing the dependence between age and levels of metabolites [45–49]. They have found an increase in NAA and Cr and a decrease in Cho and mI (Fig. 7). Rapid changes occur within the first year of life and then the rate of change declines, with final adult values being reached until about 20 years of age. Similar curves should be used with caution because they depend on their acquisition protocol. Ideally, each site should produce its own normative curves.

Brain MRS spectra also vary with anatomical location [50, 51] (Fig. 8) (Table 2). Generally Cho and NAA signals are higher in white matter than in gray matter. Conversely Cr, mI and Glx are less concentrated in white matter than in gray matter. The highest Cr and Cho values are found in the cerebellum.

In pathological cases the choice of the MRS location is also very important. In chemical shift imaging, phase shifting in k-space can be used to shift voxels in one or more dimensions to

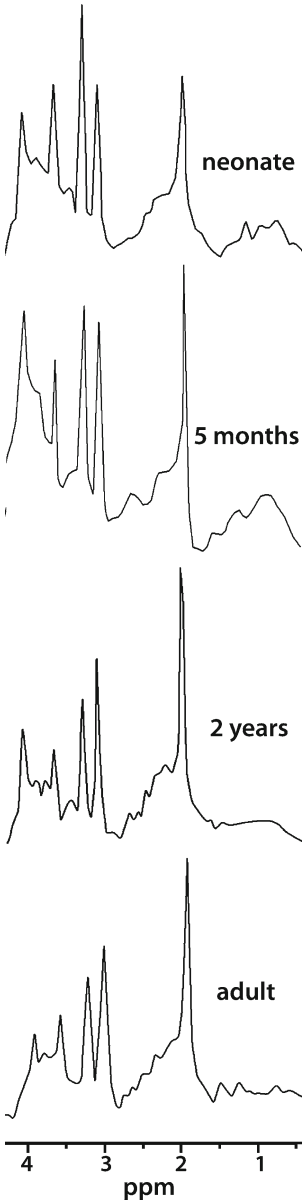


**Fig. 6** Normal age-related changes of proton spectra (TE=25 ms) from a single voxel located in the basal ganglia. *TE* echo time

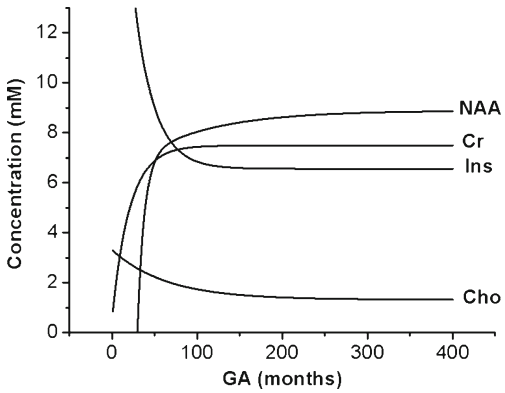


**Fig. 7** Normative magnetic resonance spectroscopy curves according to Kreis et al. [46]. *GA* gestational age

better enclose the region of interest [15]. In single-voxel techniques the placement of the voxel and its size depend on the clinical question. For example in tumors or in suspicious lesions the voxel must be placed in the center and its size has to be small enough to prevent contamination with nearby healthy tissue. Of course smaller voxels require an increased number of total scans and therefore longer acquisition times, but in cases of small lesions they give reliable and useful information. Another example is diffuse brain injury, where the single voxel must be placed to gray matter, far from blood and lesions to rule out global hypoxic injury [52–54]. Gray matter is more susceptible to the effects of glutamate excitotoxicity, the main cause of neuronal death after ischemia [55], because of the ambudance of postsynaptic glutamate receptors and increased synaptic activity. On the other hand if there is no suspicion of hypoxic injury, white matter is preferred to rule out diffuse axonal damage. Similarly in cases of severe hypoxic ischemia in both preterm and term neonates the deep gray matter nuclei are an ideal location for single-voxel MRS because of the known vulnerability of these regions to hypoxic–ischemic injury [56, 57].

## Echo time dependence

Spectra acquired with short echo times (20–35 ms) have high signal-to-noise and they allow contributions from protons with short T2 such as the myo-inositol, the Glx compounds and the lipids. However baseline distortions, originating from poorly resolved broad resonances from short T2 and J-coupled protons, perplex the interpretation and the quantification of the spectra. On the other hand, on intermediate (135–144 ms) or long (270–288 ms) echo times, spectra become less informative but simpler and easier to quantify, with better defined baseline (Fig. 9).

Spin echoes in MRS sequences are usually created with 180° refocusing pulses, which invert the spin dephasing caused by magnetic field inhomogeneous effects. These pulses do not refocus the effects of J-coupling, which results in a TE-dependent phase modulation of the spectra. The lactate doublet, especially, appears inverted at odd multiples of TE=1/J=144 ms (Fig. 4). This phenomenon can be used to highlight the inverted lactate doublet against nearby non-inverted lipid peaks.

## Field dependence

Common clinical MR systems have magnetic field strengths of 0.2–3 T. Generally, higher magnetic fields increase spin

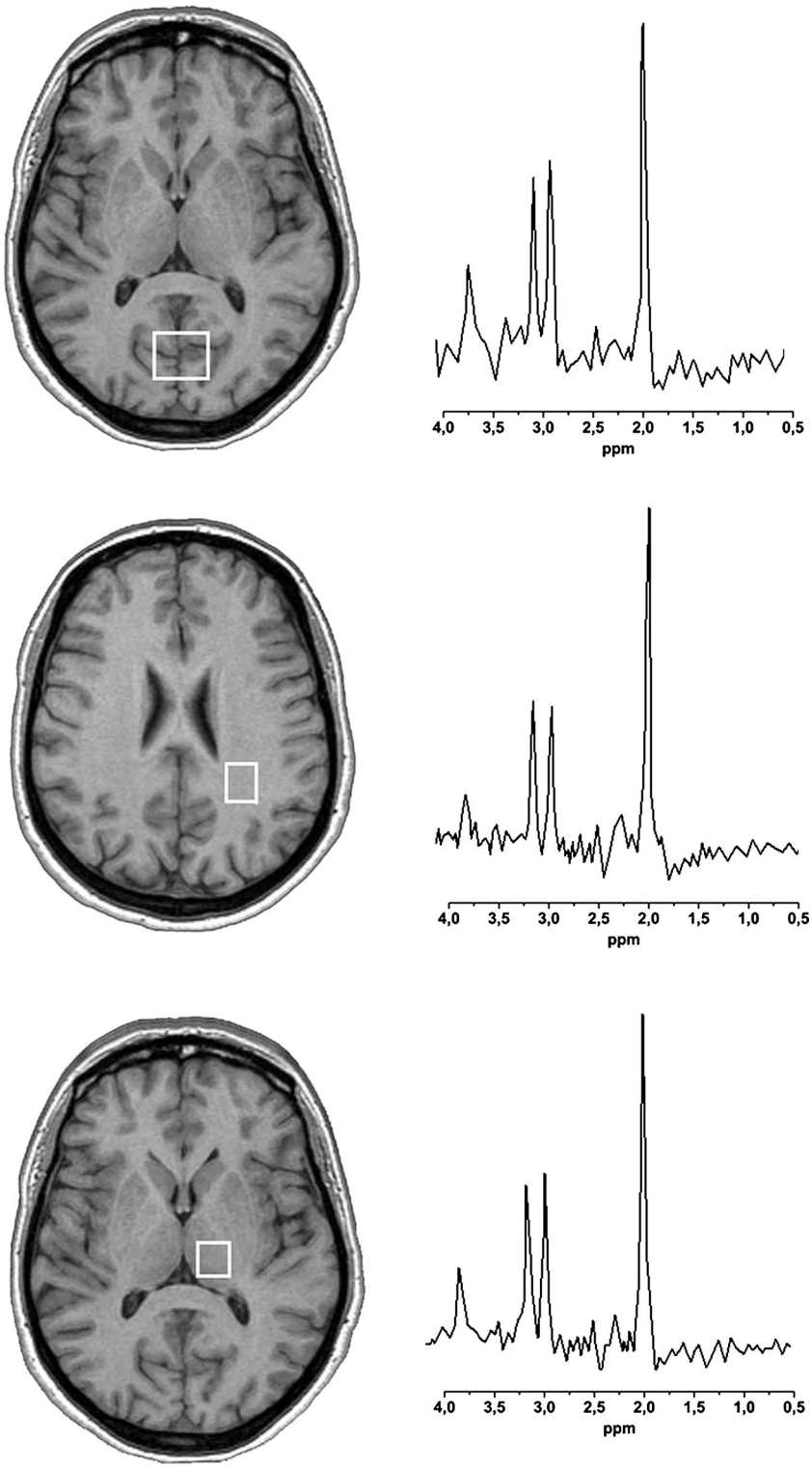


**Fig. 8** Single-voxel proton magnetic resonance spectroscopy from a 24-year-old man. *Top* is from gray matter, *middle* is from white matter, and *bottom* is from thalamus, demonstrating location dependence of magnetic resonance spectroscopy

polarization and provide better signal-to-noise ratio and increased sensitivity, creating the possibility of obtaining spectra from smaller volumes or faster acquisitions. Additionally they improve spectral resolution (i.e. chemical shift dispersion), which in turn allows for more reliable quantitation of MRS spectra and better water suppression. However, field inhomogeneities and enhanced susceptibility effects, both prominent in high fields, may

**Table 2** Age and location dependence of metabolite concentration (mean ± standard deviation in mM) obtained from single voxel STEAM pulse sequences (TE/TR =6,000/20 ms). The data are adapted from Pouwels et al. [50]

| Age | Location | Cho | Cr | NAA | mI |
|---|---|---|---|---|---|
| 0–1 year | GM | 1.4±0.3 | 5.5±0.7 | 5.8±1.0 | 4.8±0.7 |
| | WM | 2.0±0.2 | 5.4±0.5 | 5.8±0.8 | 4.0±0.5 |
| | BG | 2.0±0.1 | 7.6±0.5 | 7.4±0.5 | 3.7±0.5 |
| | Cer | 2.1±0.1 | 8.1±1.0 | 4.2±0.5 | 7.3±1.2 |
| 1–2 years | GM | 1.2±0.2 | 6.4±0.8 | 7.2±0.7 | 4.4±0.9 |
| | WM | 1.8±0.2 | 5.0±0.5 | 5.8±0.6 | 3.5±0.6 |
| | BG | 1.9±0.2 | 7.6±0.5 | 6.2±0.6 | 3.7±0.5 |
| | Cer | 1.9±0.3 | 7.8±0.6 | 4.9±0.3 | 6.6±1.2 |
| 2–5 years | GM | 1.1±0.2 | 6.4±0.7 | 8.1±0.9 | 4.7±0.4 |
| | WM | 1.9±0.2 | 5.0±0.4 | 6.2±0.7 | 3.7±0.6 |
| | BG | 1.8±0.2 | 7.9±0.6 | 7.3±1.0 | 3.8±0.9 |
| | Cer | 1.9±0.1 | 8.2±1.0 | 6.0±0.8 | 6.1±0.4 |
| 5–10 years | GM | 1.2±0.2 | 6.2±0.5 | 8.0±0.9 | 4.6±0.7 |
| | WM | 1.6±0.3 | 4.0±0.4 | 6.1±0.7 | 3.7±0.6 |
| | BG | 1.9±0.2 | 7.6±0.6 | 7.0±0.8 | 4.1±0.4 |
| | Cer | 2.1±0.3 | 8.7±0.7 | 6.2±0.7 | 5.8±0.3 |
| 10–18 years | GM | 1.1±0.2 | 6.5±0.5 | 8.9±0.8 | 4.3±0.6 |
| | WM | 1.6±0.2 | 4.8±0.4 | 6.3±0.5 | 3.9±1.2 |
| | BG | 1.8±0.4 | 7.7±0.9 | 6.1±0.8 | 3.3±0.8 |
| | Cer | 2.0±0.2 | 8.6±0.7 | 6.3±0.7 | 4.8±0.9 |

*BG* basal ganglia, *Cer* cerebellum, *Cho* choline, *Cr* creatine and phosphocreatine, *GM* gray matter, *mI* Myo-inositol, *NAA* N-acetylaspartate, *WM* white matter

produce chemical shift misregistration, distort baseline and reduce resolution and sensitivity. Moreover in higher fields relaxation times are longer and the saturation effects are larger. Overall, moving from 1.5 to 3 T can probably improve a signal-to-noise ratio at least 50%. Particular care must be given in the cases of high fields (3 T and above) at the anomalous J-modulation effect, which results in lactate signal reduction and underestimated quantification [58].

## Future of MRS

Compared to the progress of nuclear magnetic resonance in chemistry, MRS is still at its infancy. The reason lies in the challenges and hurdles imposed by the in vivo measurements. Low signal-to-noise ratio, field inhomogeneity, water suppression and localization pulses are basic MRS factors that hinder the full in vivo exploitation of the wealth of techniques in nuclear magnetic resonance. Studies have shown that improvements at 3 T and 4 T are below the theoretical predictions and increased resolution was counterbalanced by increased line widths [59, 60]. Nevertheless the gradual transition to higher magnetic fields and multi-frequency scanners is expected to boost MRS clinical value and research potential by allowing better spectral resolution and multidimensional techniques in acceptable scanning times. Already many studies have demonstrated the strength of 2-D MRS, but they remain far from the clinical field, mainly because of their long acquisition times [61, 62].

Another promising field of progress is the hyperpolarized MRS using carbon-13 ($^{13}C$) or nitrogen-15 ($^{15}N$) [63, 64]. $^{13}C$ hyperpolarized pyruvate achieved with dynamic nuclear polarization along with strong fields and low temperatures has allowed unprecedented real-time visualization of the biochemical pathways of normal and abnormal metabolism [64, 65].

MRS has an important but complementary diagnostic role and supplements the clinical examination and conventional MRI by providing specific metabolite/biochemical information. Although MRS can be considered a method of molecular imaging, its low sensitivity dictates a good knowledge of the principles and limitations of this technique when it is applied and interpreted in clinical practice.

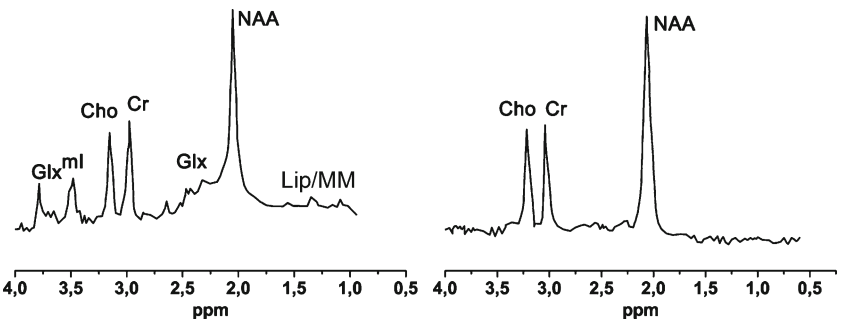


**Fig. 9** Short echo time (TE=35 ms, *left*) and long echo time (TE=144 ms, *right*) normal magnetic resonance spectroscopy proton spectrum of the white matter of a 36-year-old man. Note the absence of Glx, mI and Lip/MM in the long echo time spectrum. *Glx* glutamate and glutamine, *Lip* lipids, *mI* myo-inositol, *MM* macromolecules

**Conflicts of interest** None

## References


1. Boesch C (1999) Molecular aspects of magnetic resonance imaging and spectroscopy. Mol Aspects Med 20:185–318
2. Kwock L, Smith JK, Castillo M et al (2006) Clinical role of proton magnetic resonance spectroscopy in oncology: brain, breast, and prostate cancer. Lancet Oncol 7:859–868
3. Cecil KM, Jones BV (2001) Magnetic resonance spectroscopy of the pediatric brain. Top Magn Reson Imaging 12:435–452
4. Dezortova M, Hajek M (2008) (1)H MR spectroscopy in pediatrics. Eur J Radiol 67:240–249
5. Gillard JH, Waldman AD, Barker PB (2005) Clinical MR neuroimaging: diffusion, perfusion and spectroscopy. Cambridge University Press, Cambridge
6. Tzika AA (2008) Proton magnetic resonance spectroscopic imaging as a cancer biomarker for pediatric brain tumors (review). Int J Oncol 32:517–526
7. Cecil KM (2006) MR spectroscopy of metabolic disorders. Neuroimaging Clin N Am 16:87–116
8. Dong Z, Dreher W, Leibfritz D (2006) Toward quantitative short-echo-time in vivo proton MR spectroscopy without water suppression. Magn Reson Med 55:1441–1446
9. Haase A, Frahm J, Hanicke W et al (1985) 1H NMR chemical shift selective (CHESS) imaging. Phys Med Biol 30:341–344
10. Moonen C, van Zijl P (1990) Highly effective water suppression for in vivo proton NMR spectroscopy (DRYSTEAM). J Magn Reson 88: 28–41
11. Gupta R (1976) Dynamic range problem in fourier transform NMR. Modified WEFT pulse sequence. J Magn Reson 24:461–465
12. Keevil SF (2006) Spatial localization in nuclear magnetic resonance spectroscopy. Phys Med Biol 51:R579–R636
13. Brown TR, Kincaid BM, Ugurbil K (1982) NMR chemical shift imaging in three dimensions. Proc Natl Acad Sci U S A 79:3523–3526
14. Maudsley A, Hilal S, Perman W et al (1983) Spatially resolved high-resolution spectroscopy by 'four-dimensional' NMR. J Magn Reson 51:147–152
15. Skoch A, Jiru F, Bunke J (2008) Spectroscopic imaging: basic principles. Eur J Radiol 67:230–239
16. Duijn J, Matson G, Maudsley A et al (1992) 3D phase encoding 1H spectroscopic imaging of human brain. Magn Reson Imaging 10: 315–319
17. Moonen C, Sobering G, van Zijl P et al (1992) Proton spectroscopic imaging of human brain. J Magn Reson 98:556–575
18. Posse S, Schuknecht B, Smith ME et al (1993) Short echo time proton MR spectroscopic imaging. J Comput Assist Tomogr 17:1–14
19. Poullet J-B, Sima DM, Van Huffel S (2008) MRS signal quantitation: a review of time- and frequency-domain methods. J Magn Reson 195:134–144
20. Jansen JF, Backes WH, Nicolay K et al (2006) 1H MR spectroscopy of the brain: absolute quantification of metabolites. Radiology 240: 318–332
21. Alger JR (2010) Quantitative proton magnetic resonance spectroscopy and spectroscopic imaging of the brain: a didactic review. Top Magn Reson Imaging 21:115–128
22. Joliot M, Mazoyer BM, Huesman RH (1991) In vivo NMR spectral parameter estimation: a comparison between time and frequency domain methods. Magn Reson Med 18:358–370
23. Henriksen O (1995) In vivo quantitation of metabolite concentrations in the brain by means of proton MRS. NMR Biomed 8:139–148
24. Naressi A, Couturier C, Castang I et al (2001) Java-based graphical user interface for MRUI, a software package for quantitation of in vivo/medical magnetic resonance spectroscopy signals. Comput Biol Med 31:269–286
25. Steffen-Smith EA, Venzon DJ, Bent RS et al (2012) Single- and multivoxel proton spectroscopy in pediatric patients with diffuse intrinsic pontine glioma. Int J Radiat Oncol Biol Phys 84:774–779
26. Kadri M, Shu S, Holshouser B et al (2003) Proton magnetic resonance spectroscopy improves outcome prediction in perinatal CNS insults. J Perinatol 23:181–185
27. Martin WR (2007) MR spectroscopy in neurodegenerative disease. Mol Imaging Biol 9:196–203
28. Astrakas LG, Zurakowski D, Tzika AA et al (2004) Noninvasive magnetic resonance spectroscopic imaging biomarkers to predict the clinical grade of pediatric brain tumors. Clin Cancer Res 10:8220–8228
29. Baslow MH, Suckow RF, Gaynor K et al (2003) Brain damage results in down-regulation of N-acetylaspartate as a neuronal osmolyte. NeuroMolecular Med 3:95–104
30. Glunde K, Bhujwalla ZM, Ronen SM (2011) Choline metabolism in malignant transformation. Nat Rev Cancer 11:835–848
31. Wang ZJ, Zimmerman RA (1998) Proton MR spectroscopy of pediatric brain metabolic disorders. Neuroimaging Clin N Am 8:781–807
32. Zarifi MK, Astrakas LG, Poussaint TY et al (2002) Prediction of adverse outcome with cerebral lactate level and apparent diffusion coefficient in infants with perinatal asphyxia. Radiology 225:859–870
33. Lin DD, Crawford TO, Barker PB (2003) Proton MR spectroscopy in the diagnostic evaluation of suspected mitochondrial disease. AJNR Am J Neuroradiol 24:33–41
34. Gillard JH, Barker PB, van Zijl PC et al (1996) Proton MR spectroscopy in acute middle cerebral artery stroke. AJNR Am J Neuroradiol 17:873–886
35. Bulik M, Jancalek R, Vanicek J et al (2013) Potential of MR spectroscopy for assessment of glioma grading. Clin Neurol Neurosurg 115:146–153
36. Lai PH, Ho JT, Chen WL et al (2002) Brain abscess and necrotic brain tumor: discrimination with proton MR spectroscopy and diffusion-weighted imaging. AJNR Am J Neuroradiol 23:1369–1377
37. Wang ZJ, Vigneron DB, Miller SP et al (2008) Brain metabolite levels assessed by lactate-edited MR spectroscopy in premature neonates with and without pentobarbital sedation. AJNR Am J Neuroradiol 29:798–801
38. Ashwal S, Holshouser B, Tong K et al (2004) Proton spectroscopy detected myoinositol in children with traumatic brain injury. Pediatr Res 56:630–638
39. Shonk TK, Moats RA, Gifford P et al (1995) Probable Alzheimer disease: diagnosis with proton MR spectroscopy. Radiology 195: 65–72
40. Adibhatla RM, Hatcher JF, Dempsey RJ (2006) Lipids and lipidomics in brain injury and diseases. AAPS J 8:E314–E321
41. Wootton-Gorges SL, Buonocore MH, Kuppermann N et al (2005) Detection of cerebral {beta}-hydroxy butyrate, acetoacetate, and lactate on proton MR spectroscopy in children with diabetic ketoacidosis. AJNR Am J Neuroradiol 26:1286–1291
42. Leuzzi V, Bianchi MC, Tosetti M et al (2000) Clinical significance of brain phenylalanine concentration assessed by in vivo proton magnetic resonance spectroscopy in phenylketonuria. J Inherit Metab Dis 23:563–570
43. Burtscher IM, Holtas S (1999) In vivo proton MR spectroscopy of untreated and treated brain abscesses. AJNR Am J Neuroradiol 20: 1049–1053
44. Panigrahy A, Krieger MD, Gonzalez-Gomez I et al (2006) Quantitative short echo time 1H-MR spectroscopy of untreated pediatric brain tumors: preoperative diagnosis and characterization. AJNR Am J Neuroradiol 27:560–572

45. Kreis R, Hofmann L, Kuhlmann B et al (2002) Brain metabolite composition during early human brain development as measured by quantitative in vivo 1H magnetic resonance spectroscopy. Magn Reson Med 48:949–958
46. Kreis R, Ernst T, Ross BD (1993) Development of the human brain: in vivo quantification of metabolite and water content with proton magnetic resonance spectroscopy. Magn Reson Med 30: 424–437
47. Toft PB, Leth H, Lou HC et al (1994) Metabolite concentrations in the developing brain estimated with proton MR spectroscopy. J Magn Reson Imaging 4:674–680
48. Kok RD, van den Berg PP, van den Bergh AJ et al (2002) Maturation of the human fetal brain as observed by 1H MR spectroscopy. Magn Reson Med 48:611–616
49. Horska A, Kaufmann WE, Brant LJ et al (2002) In vivo quantitative proton MRSI study of brain development from childhood to adolescence. J Magn Reson Imaging 15:137–143
50. Pouwels PJ, Frahm J (1998) Regional metabolite concentrations in human brain as determined by quantitative localized proton MRS. Magn Reson Med 39:53–60
51. Pouwels PJ, Brockmann K, Kruse B et al (1999) Regional age dependence of human brain metabolites from infancy to adulthood as detected by quantitative localized proton MRS. Pediatr Res 46: 474–485
52. Ashwal S, Tong KA, Ghosh N et al. (2014) Application of advanced neuroimaging modalities in pediatric traumatic brain injury. J Child Neurol [Epub ahead of print]
53. Granacher RP (2008) Traumatic brain injury: methods for clinical and forensic neuropsychiatric assessment. CRC Press/Taylor & Francis Group, Boca Raton
54. Ross B, Bluml S (2001) Magnetic resonance spectroscopy of the human brain. Anat Rec 265:54–84
55. Ankarcrona M, Dypbukt JM, Bonfoco E et al (1995) Glutamate-induced neuronal death: a succession of necrosis or apoptosis depending on mitochondrial function. Neuron 15:961–973
56. Huang BY, Castillo M (2008) Hypoxic-ischemic brain injury: imaging findings from birth to adulthood. Radiographics 28:417–439, quiz 617
57. Johnston MV (1995) Neurotransmitters and vulnerability of the developing brain. Brain Dev 17:301–306
58. Liu HS, Chung HW, Juan CJ et al (2008) Anomalous J-modulation effects on amino acids in clinical 3T MR spectroscopy. AJNR Am J Neuroradiol 29:1644–1648
59. Kim JH, Chang KH, Na DG et al (2006) Comparison of 1.5T and 3T 1H MR spectroscopy for human brain tumors. Korean J Radiol 7: 156–161
60. Inglese M, Spindler M, Babb JS et al (2006) Field, coil, and echo-time influence on sensitivity and reproducibility of brain proton MR spectroscopy. AJNR Am J Neuroradiol 27:684–688
61. Thomas MA, Hattori N, Umeda M et al (2003) Evaluation of two-dimensional L-COSY and JPRESS using a 3T MRI scanner: from phantoms to human brain in vivo. NMR Biomed 16:245–251
62. Nagarajan R, Sarma MK, Thames AD et al (2012) 2D MR spectroscopy combined with prior-knowledge fitting is sensitive to HCV-associated cerebral metabolic abnormalities. Int J Hepatol 2012: 179365
63. Cudalbu C, Comment A, Kurdzesau F et al (2010) Feasibility of in vivo 15N MRS detection of hyperpolarized 15N labeled choline in rats. Phys Chem Chem Phys 12:5818–5823
64. Ross BD, Bhattacharya P, Wagner S et al (2010) Hyperpolarized MR imaging: neurologic applications of hyperpolarized metabolism. AJNR Am J Neuroradiol 31:24–33
65. Rowland IJ, Peterson ET, Gordon JW et al (2010) Hyperpolarized 13carbon MR. Curr Pharm Biotechnol 11:709–719